iScience

CellPress
OPEN ACCESS

Article

The inactivation of *tolC* sensitizes *Escherichia coli* to perturbations in lipopolysaccharide transport

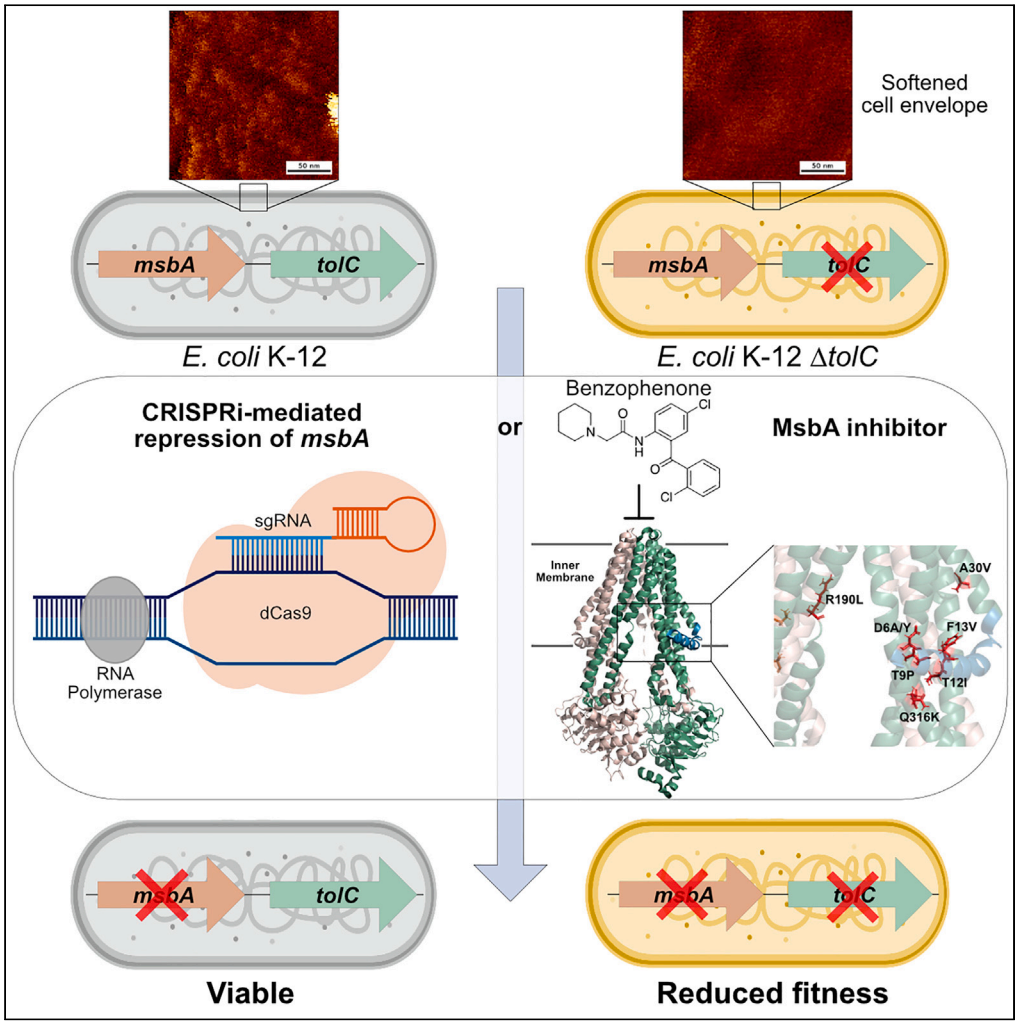

Shawna Zhu, Mary Kate Alexander, Telmo O. Paiva, ..., Yves F. Dufrêne, Eric D. Brown, Georgina Cox

gcox@uoguelph.ca

Highlights

tolC null mutants are sensitized to structurally unrelated MsbA inhibitors

A synthetic-sick interaction exists between *tolC* and *msbA*

The benzophenones represent a distinct class of MsbA inhibitors

Inactivating *tolC* induces cell envelope softening and increased permeability

Zhu et al., iScience *27*, 109592
May 17, 2024
https://doi.org/10.1016/j.isci.2024.109592

iScience

CellPress
OPEN ACCESS

Article

The inactivation of *tolC* sensitizes *Escherichia coli* to perturbations in lipopolysaccharide transport

Shawna Zhu,[1] Mary Kate Alexander,[2] Telmo O. Paiva,[3] Kenneth Rachwalski,[4] Anh Miu,[5] Yiming Xu,[2] Vishal Verma,[6] Mike Reichelt,[7] Yves F. Dufrêne,[3] Eric D. Brown,[4] and Georgina Cox[1,8,*]

SUMMARY

The *Escherichia coli* outer membrane channel TolC complexes with several inner membrane efflux pumps to export compounds across the cell envelope. All components of these complexes are essential for robust efflux activity, yet *E. coli* is more sensitive to antimicrobial compounds when *tolC* is inactivated compared to the inactivation of genes encoding the inner membrane drug efflux pumps. While investigating these susceptibility differences, we identified a distinct class of inhibitors targeting the core-lipopolysaccharide translocase, MsbA. We show that *tolC* null mutants are sensitized to structurally unrelated MsbA inhibitors and *msbA* knockdown, highlighting a synthetic-sick interaction. Phenotypic profiling revealed that *tolC* inactivation induced cell envelope softening and increased outer membrane permeability. Overall, this work identified a chemical probe of MsbA, revealed that *tolC* is associated with cell envelope mechanics and integrity, and highlighted that these findings should be considered when using *tolC* null mutants to study efflux deficiency.

INTRODUCTION

Diderm bacteria represent a unique challenge for compound permeation and transport since they possess two membranes with orthogonal properties.[1] In *Escherichia coli*, the inner membrane (IM) is a phospholipid bilayer permeable to amphiphilic and hydrophobic compounds yet restrictive to polar and highly charged.[2,3] In contrast, the outer membrane (OM) is atypical, with an unusual asymmetric lipid distribution that impedes entry; the outer leaflet comprises lipopolysaccharide (LPS) and the inner leaflet phospholipids.[1] Polyanionic LPS molecules are often bridged by lateral interactions with divalent cations, imparting integrity to the OM and reducing the permeation of large and hydrophobic compounds.[1] Small hydrophilic compounds can diffuse through the OM via the OmpA, OmpF, and OmpC porins, which form a relatively static network.[4] OM proteins such as OmpA, Braun's lipoprotein (Lpp), and peptidoglycan lipoprotein (Pal) stabilize the OM through interactions with the peptidoglycan.[1] In addition to the barrier functions of the OM, this structure provides physical strength to the cell envelope, compensating for the relatively thin layer of peptidoglycan in gram-negative bacteria.[5] The OM also plays a role in determining the shape of *E. coli*.[6]

Importantly, the impermeable nature of the OM augments the exporting activities of drug efflux pumps, which collectively render *E. coli* intrinsically resistant to a broad spectrum of antimicrobial agents.[2,7] In *E. coli*, an extensive network of conserved drug efflux pumps contributes to antimicrobial detoxification, and these proteins can be broadly categorized into two main groups: (1) single-component efflux pumps residing in the IM and (2) multicomponent drug efflux systems that span the entire cell envelope.[8] The latter comprises an efflux pump driving export from the IM, periplasmic adaptor proteins, and a nonspecific OM channel for transport across the OM. Eight different *E. coli* efflux pumps are known to complex with the OM channel TolC,[9] and *tolC* null mutants are commonly used efflux-deficient strains that display increased sensitivity to a wide variety of antimicrobial agents.[10] TolC is associated with several other cellular functions, including metabolite extrusion and acid tolerance.[11] Additionally, the protein serves as a component of type I secretion systems, enabling virulence factor secretion.[11]

We recently reported the generation of a mutant strain, Efflux KnockOut-35: EKO-35, lacking 35 IM efflux pumps comprising the *E. coli* drug efflux network, including all pumps complexing with TolC.[9] We anticipated EKO-35 would be equally, if not more, susceptible to

[1]College of Biological Sciences, Department of Molecular and Cellular Biology, University of Guelph, 50 Stone Road E, Guelph, ON N1G 2W1, Canada
[2]Genentech Inc, Infectious Diseases, South San Francisco, CA, USA
[3]Institute of Life Sciences, UCLouvain, Croix du Sud, 4-5, bte L7.07.06, B-1348 Louvain-la-Neuve, Belgium
[4]Biochemistry and Biomedical Sciences and Degroote Institute for Infectious Disease Research, McMaster University, Hamilton, ON L8S 4L8, Canada
[5]Genentech Inc, Biochemical and Cellular Pharmacology, South San Francisco, CA, USA
[6]Genentech Inc, Discovery Chemistry, South San Francisco, CA, USA
[7]Genentech Inc, Pathology, South San Francisco, CA, USA
[8]Lead contact
*Correspondence: gcox@uoguelph.ca
https://doi.org/10.1016/j.isci.2024.109592

antimicrobial agents than a *tolC* null mutant (harboring an in-frame marker-less deletion) since this strain lacks all efflux pumps complexing with TolC and all single-component efflux pumps. Unexpectedly, while both strains were highly susceptible to a broad range of antimicrobials, the Δ*tolC* mutant was more susceptible than EKO-35 in several instances.[9]

Here, we explored the mechanistic basis of these susceptibility differences, identifying an inhibitor of MsbA, the ATP-binding cassette (ABC) transporter responsible for "flipping" core-LPS to the periplasmic leaflet of the IM.[1] We subsequently uncovered a synthetic-sick interaction between *msbA* and *tolC* and revealed that the cell envelope of Δ*tolC* exhibits softening and increased permeability, which does not appear to be associated with known drug efflux pumps that form complexes with this OM channel. Collectively, this work reveals that *tolC* inactivation sensitizes *E. coli* to perturbations in LPS transport and impacts cell envelope mechanics and integrity. Our findings highlight that these factors should be considered when using *tolC* mutants to study efflux since increased sensitivity is not necessarily attributable to decreased efflux. Furthermore, we propose that the *tolC*-associated synthetic-sick interaction could be exploited to identify new cell envelope biogenesis machinery inhibitors.

RESULTS

Exploring the mechanistic basis of antimicrobial susceptibility differences observed between efflux-deficient strains

As described, we reported susceptibility differences between efflux-deficient *E. coli* K-12 (BW25113) strains, Δ*tolC* and EKO-35, despite the latter lacking the IM efflux pumps that complex with TolC.[9] Compared to EKO-35, we reasoned that a mutant lacking only the IM efflux pumps complexing with TolC would be a more suitable comparison to a *tolC* null mutant since single-component efflux pumps are still produced. Therefore, using a combination of λ-Red recombineering and CRISPR-Cas9-mediated counter selection, here we inactivated eight genes (*acrB*, *acrD*, *acrE*, *mdtF*, *mdtB*, *emrY*, *emrB*, *macB*) encoding efflux pumps that complex with TolC in *E. coli* K-12 (BW25113),[12] generating the tripartite efflux (TE) mutant. Three non-synonymous mutations, identified via long-read next-generation sequencing, were repaired in the TE mutant to ensure they were not responsible for antimicrobial susceptibility differences (Table S1). Finally, Illumina sequencing confirmed that the repaired TE mutant and Δ*tolC* were isogenic except for disruptions in the efflux-associated genes, as expected (Table S1).

Susceptibility testing revealed that both efflux-deficient strains exhibited increased sensitivity to a broad range of antimicrobial agents (Figure S1; Table S2); however, while Δ*tolC* was highly sensitized to several of the uncharacterized synthetic antimicrobial compounds,[9] the TE mutant exhibited high-level resistance, consistent with our previous study using the EKO-35 efflux-deficient strain (Figure 1A; Table S2). In most cases, increasing OM permeability by introducing a non-selective FhuA-derivatized pore[9,10,13] did not impact these susceptibility differences, suggesting they are not solely attributable to increased OM permeability in Δ*tolC* (Figure 1A).

tolC inactivation sensitizes *E. coli* to MsbA inhibition

To gain insight into the mechanistic basis of this phenomenon, we next sought to generate spontaneous mutations conferring resistance to the synthetic compounds with increased Δ*tolC* activity (Figure 1A). In the presence of a benzophenone compound, synthetic compound #20 (syn. #20), suppressor mutations in Δ*tolC* emerged at a frequency of 1.1×10^{-7}. Next-generation sequencing of different spontaneous mutants identified several nonsynonymous mutations that localized to the *msbA* gene, and these amino acid substitutions clustered within the same region of the protein (Figure 1B). All the suppressor mutants exhibited high-level resistance to the benzophenone compound, with >16-fold increases in the minimum inhibitory concentrations (MICs) (Table 1).

To further investigate whether MsbA was the target, we assessed the effect of target gene overexpression and knockdown. Consistent with MsbA being the target of the benzophenone, the overexpression of *msbA* in Δ*tolC* (pGDP2:*msbA*) conferred high-level resistance (>16-fold increase in the MIC) (Table 1). Additionally, CRISPR interference (CRISPRi)-mediated *msbA* knockdown, confirmed using real-time quantitative reverse-transcription PCR (Figure S2), further sensitized Δ*tolC*, increasing sensitivity >64-fold (Table 1). Additionally, the wild-type and TE mutant strains were sensitized to syn. #20 when *msbA* levels were reduced (Table 1).

Finally, *tolC* was disrupted in the TE mutant using CRISPR-Cas9-mediated counterselection and the introduction of three tandem stop codons, which increased the susceptibility of the TE mutant to the same level as the Δ*tolC* mutant, revealing that the syn. #20 susceptibility differences are directly associated with TolC (Table 1).

MsbA is an essential translocase that "flips" nascent LPS to the outer leaflet of the IM; as such, the protein is an attractive antibacterial target.[14–16] There are two known classes of MsbA inhibitors: tetrahydrobenzothiophene 1 (TBT-1)[17] and a quinoline-containing compound series.[18,19] To further probe the relationship between TolC and MsbA, we conducted susceptibility testing with members of the quinoline series (G332 and G913), revealing that Δ*tolC* was also hypersensitized to these structurally dissimilar MsbA inhibitors compared to the TE mutant (Figure 1C; Table 1).

Taken together, these data indicate that the benzophenone compound likely targets MsbA and highlights a striking association between *tolC* and MsbA, which appears to be distinct from the drug efflux pumps known to form complexes with this OM channel.

The benzophenones represent a distinct class of MsbA inhibitors

To further substantiate MsbA as the target of the benzophenone compound, ATPase inhibition was assessed using purified MsbA reconstituted into amphipols, as previously described.[18,19] The compound exhibited dose-dependent MsbA inhibition, with a half-maximum inhibitory concentration of 0.24 μM (Figure 2A), which was comparable to the minimum inhibitory concentration in Δ*tolC* (0.80 μM). We then profiled benzophenone analogs, revealing similar activity against *E. coli* MsbA. Yet, we did not identify any compounds with increased potency in

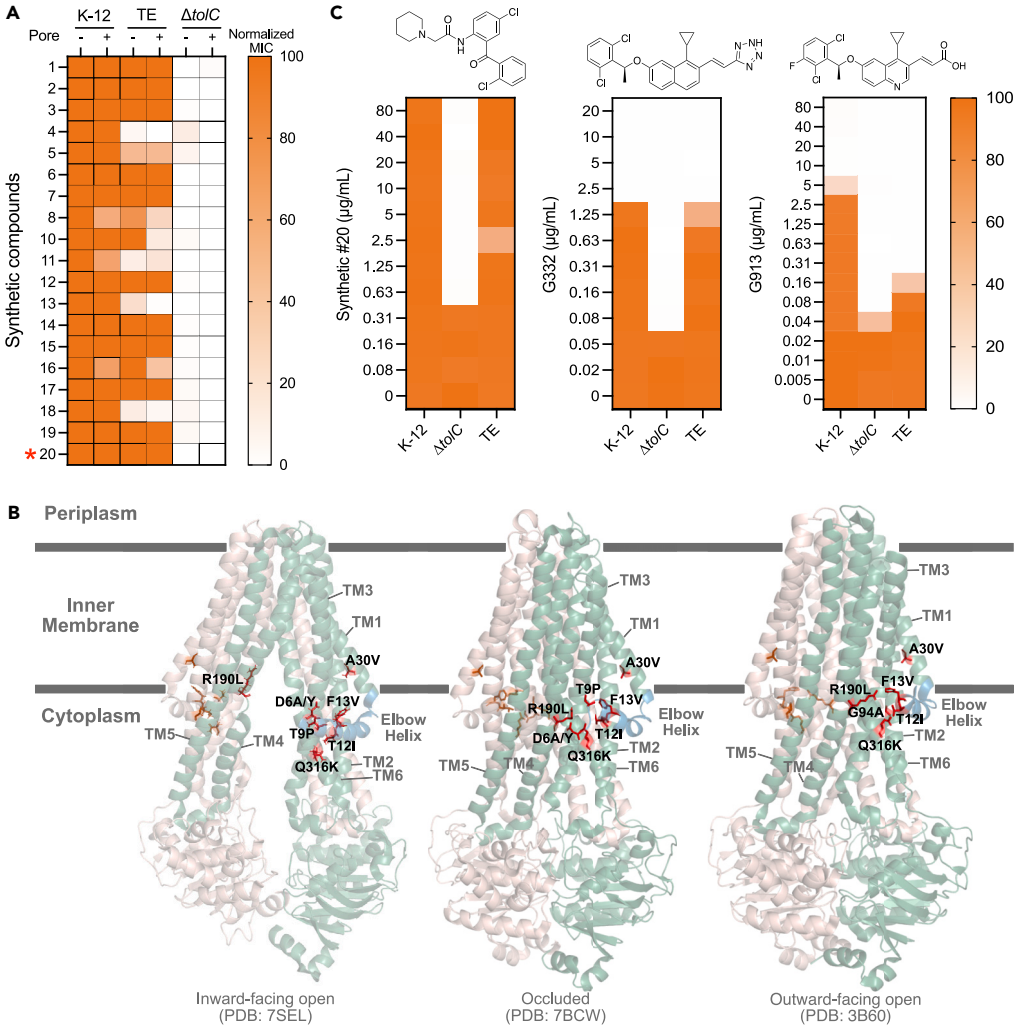

Figure 1. The inactivation of *tolC* impacts antimicrobial sensitivity differently than the disruption of genes encoding inner membrane efflux pumps

(A) Heatmap depicting the susceptibility of unporinated (–) and porinated (+) wild-type *E. coli* K-12, TE mutant, and Δ*tolC* strains to a series of synthetic compounds. The minimum inhibitory concentration (MIC) values were $\log_2$ transformed and normalized to 100% for each compound tested, where orange on the heatmap represents the highest value and white represents the lowest value.

(B) Spontaneous mutations conferring resistance in Δ*tolC* to synthetic compound #20 (labeled with a red asterisk in panel (A)). The amino acid mutations localized to or near the MsbA elbow helix (labeled and colored light blue). Three different MsbA conformations are shown: the inward-facing open (PDB ID: 7SEL), occluded (PDB ID: 7BCW), and outward-facing open conformation (PDB ID: 3B60). The protomers of MsbA are colored pink and green, with the mutations highlighted in red. TM, transmembrane helix.

(C) Susceptibility testing of the quinoline MsbA inhibitors against the K-12, Δ*tolC*, and TE mutant strains. The chemical structures of each MsbA inhibitor are shown. Growth was normalized to 100%, where orange represents the greatest OD_{600nm} and white represents the lowest OD_{600nm}. Related to Table 1.

the biochemical assay (Figure 2B). Attempts to replace the biaryl ketone reduced the activity of these compounds, highlighting the importance of this moiety (Figure S3). While the benzophenones exhibit poor antibacterial activity against wild-type *E. coli* strains, increased activity was observed against *E. coli* expressing the *imp4213* allele of *lptD*[19,20] (Table S3), enabling phenotypic analysis. The benzophenones induced membrane defects with vesicle-like invaginations due to core-LPS accumulation (Figure 2C), consistent with the phenotypes observed with the quinoline class of MsbA inhibitors and an arabinose-inducible conditional knockout of *msbA*.[19]

The benzophenones are structurally distinct from other described MsbA inhibitors, which bind to the transmembrane regions of this protein.[18,19,21,22] In contrast, the nonsynonymous resistance-conferring mutations identified within this study localized within or adjacent to the MsbA cytoplasmic elbow helices running parallel to the plane of the IM, a region of the protein that is proposed to facilitate ligand entry (Figure 1B).[23,24] In addition to recognizing physiological lipid substrates, MsbA is proposed to interact with drugs such as daunorubicin,[23,25–27] and the daunorubicin-binding site is proposed to localize near the elbow helices.[23] However, a chequerboard assay revealed no interactions between the benzophenones and daunorubicin (Figure S4A). In contrast, additive effects were observed between the benzophenones and a

Table 1. MsbA inhibitor susceptibility testing

Strain	Pore	MsbA inhibitor	Class	MIC (μg/mL)	Fold change
K-12	–	Synthetic compound #20	Benzophenone	>80	>256
Δ*tolC*	–	Synthetic compound #20	Benzophenone	0.3125	–
EKO-35	–	Synthetic compound #20	Benzophenone	>80	>256
TE	–	Synthetic compound #20	Benzophenone	>80	>256
TE + *tolC* disrupted (insertion of 3 tandem stop codons)	–	Synthetic compound #20	Benzophenone	0.3125	1
K-12	+	Synthetic compound #20	Benzophenone	>80	>256
Δ*tolC*	+	Synthetic compound #20	Benzophenone	0.3125	1
EKO-35	+	Synthetic compound #20	Benzophenone	>80	>256
TE	+	Synthetic compound #20	Benzophenone	>80	>256
Δ*bamB*	–	Synthetic compound #20	Benzophenone	>5	>16
Δ*bamB* Δ*tolC*	–	Synthetic compound #20	Benzophenone	0.3125	1
Spontaneous suppressor mutants					
Δ*tolC* $MsbA_{A30V}$	–	Synthetic compound #20	Benzophenone	>5	>16
Δ*tolC* $MsbA_{F13V}$	–	Synthetic compound #20	Benzophenone	>5	>16
Δ*tolC* $MsbA_{G94A}$	–	Synthetic compound #20	Benzophenone	>5	>16
Δ*tolC* $MsbA_{D6Y}$	–	Synthetic compound #20	Benzophenone	>5	>16
Δ*tolC* $MsbA_{D6A}$	–	Synthetic compound #20	Benzophenone	>5	>16
Target overexpression and knockdown					
Δ*tolC* pGDP2	–	Synthetic compound #20	Benzophenone	0.3125	1
Δ*tolC* pGDP2:*msbA*	–	Synthetic compound #20	Benzophenone	>5	>16
K-12 Empty vector CRISPRi	–	Synthetic compound #20	Benzophenone	>5	>16
K-12 msbA CRISPRi	–	Synthetic compound #20	Benzophenone	5	16
Δ*tolC* Empty vector CRISPRi	–	Synthetic compound #20	Benzophenone	0.3125	1
Δ*tolC msbA* CRISPRi	–	Synthetic compound #20	Benzophenone	0.0049	−64
TE Empty vector CRISPRi	–	Synthetic compound #20	Benzophenone	>5	>16
TE msbA CRISPRi	–	Synthetic compound #20	Benzophenone	5	16
Other MsbA inhibitors					
K-12	–	G717	Benzophenone	>80	>128
Δ*tolC*	–	G717	Benzophenone	0.625	–
TE	–	G717	Benzophenone	>80	>128
K-12	–	G662	Benzophenone	>40	>32
Δ*tolC*	–	G662	Benzophenone	1.25	–
TE	–	G662	Benzophenone	>40	>32
K-12	+	G662	Benzophenone	>40	>32
Δ*bamB*	–	G662	Benzophenone	>40	>32
K-12	–	G615	Benzophenone	>80	>256
Δ*tolC*	–	G615	Benzophenone	0.3125	–
TE	–	G615	Benzophenone	1.25	4
K-12	–	G332	Quinoline	2.5	32
Δ*tolC*	–	G332	Quinoline	0.0781	–
TE	–	G332	Quinoline	1.25	16
Δ*tolC* $MsbA_{A30V}$	–	G332	Quinoline	0.0391	−2
Δ*tolC* $MsbA_{F13V}$	–	G332	Quinoline	0.1563	2
Δ*tolC* $MsbA_{G94A}$	–	G332	Quinoline	0.0781	1

(*Continued on next page*)

Table 1. *Continued*

Strain	Pore	MsbA inhibitor	Class	MIC (μg/mL)	Fold change
Δ*tolC* $MsbA_{Q316K}$	–	G332	Quinoline	0.0391	−2
Δ*tolC* $MsbA_{D6A}$	–	G332	Quinoline	0.0195	−4
Δ*tolC* $MsbA_{R190L}$	–	G332	Quinoline	0.0781	1
K-12	–	G913	Quinoline	10	128
Δ*tolC*	–	G913	Quinoline	0.0781	–
TE	–	G913	Quinoline	0.3125	4
Δ*tolC* $MsbA_{A30V}$	–	G913	Quinoline	0.0391	−2
Δ*tolC* $MsbA_{F13V}$	–	G913	Quinoline	0.1563	2
Δ*tolC* $MsbA_{G94A}$	–	G913	Quinoline	0.0781	1
Δ*tolC* $MsbA_{Q316K}$	–	G913	Quinoline	0.0391	−2
Δ*tolC* $MsbA_{D6A}$	–	G913	Quinoline	0.0195	−4
Δ*tolC* $MsbA_{R190L}$	–	G913	Quinoline	0.0781	1

Strains were assessed in technical triplicate. For each strain, the minimum inhibitory concentration (MIC) values were compared to the Δ*tolC* mutant to determine the fold change. Pore, *fhuA ΔC/Δ4L*, representing a permeabilized outer membrane; K-12, the wild-type strain; Δ*tolC*, *tolC* inactivated mutant; EKO-35, Efflux KnockOut 35 mutant; TE, Tripartite Efflux mutant.

quinoline MsbA inhibitor (Figures S4B and S4C), supporting MsbA inhibition via the benzophenone and revealing that the binding mode and inhibitory actions of the two inhibitor types are not antagonistic or synergistic. Additionally, the mutations conferring resistance to the benzophenones (Figure 1B) did not provide cross-resistance to the quinolines (Table 1).

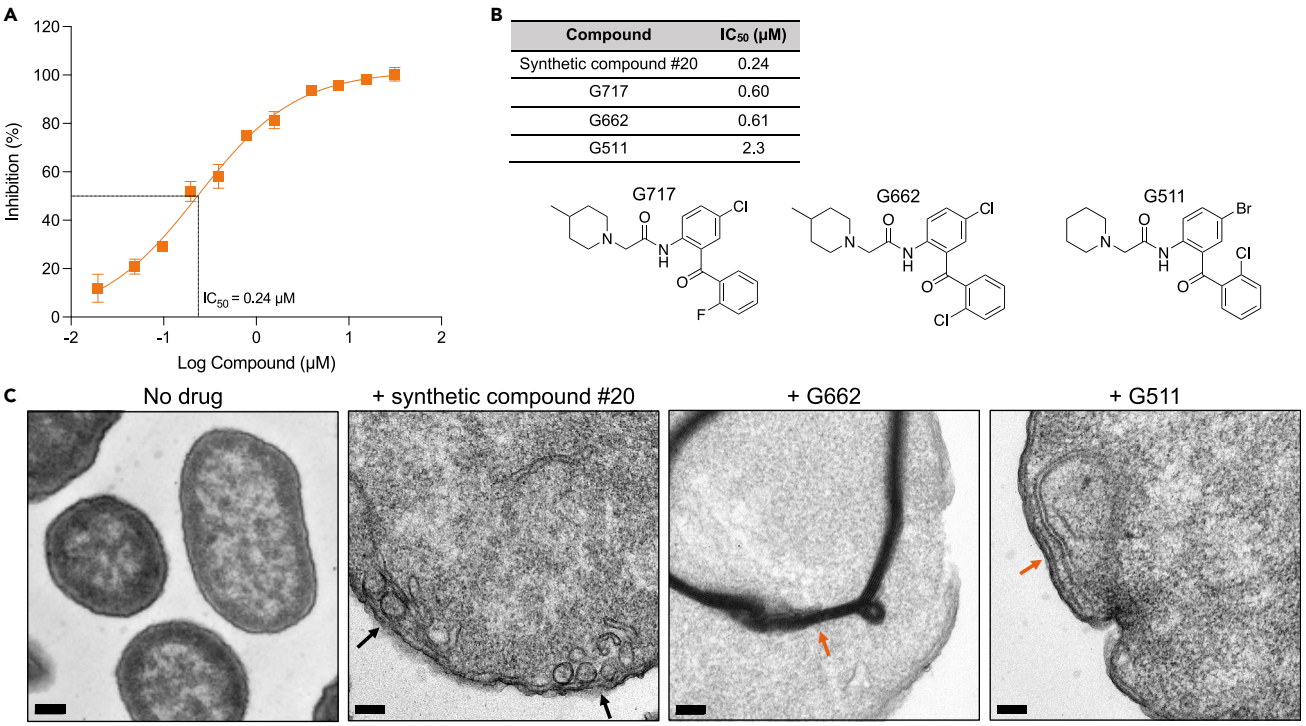

Figure 2. Biochemical and phenotypic characterization of the benzophenone MsbA inhibitors

(A) Synthetic #20 dose-response curve showing inhibition of MsbA-ATPase activity using purified *E. coli* MsbA reconstituted into amphipols. Data points represent the average ± standard deviation of three independent replicates.

(B) Benzophenone analogs exhibit comparable activity to synthetic compound #20.

(C) Representative thin-section transmission electron micrographs of strain CFT073 *lptD* (*imp4213*) treated with 20 μM of each inhibitor for 3 h. Black arrows indicate areas of vesicle-like formations of the IM, and orange arrows indicate membrane stacking due to LPS accumulation. Indentations of the cell envelope were also observed in some cells. The scale bar represents 0.2 μm for the untreated cells and 0.1 μm for the treated cells.

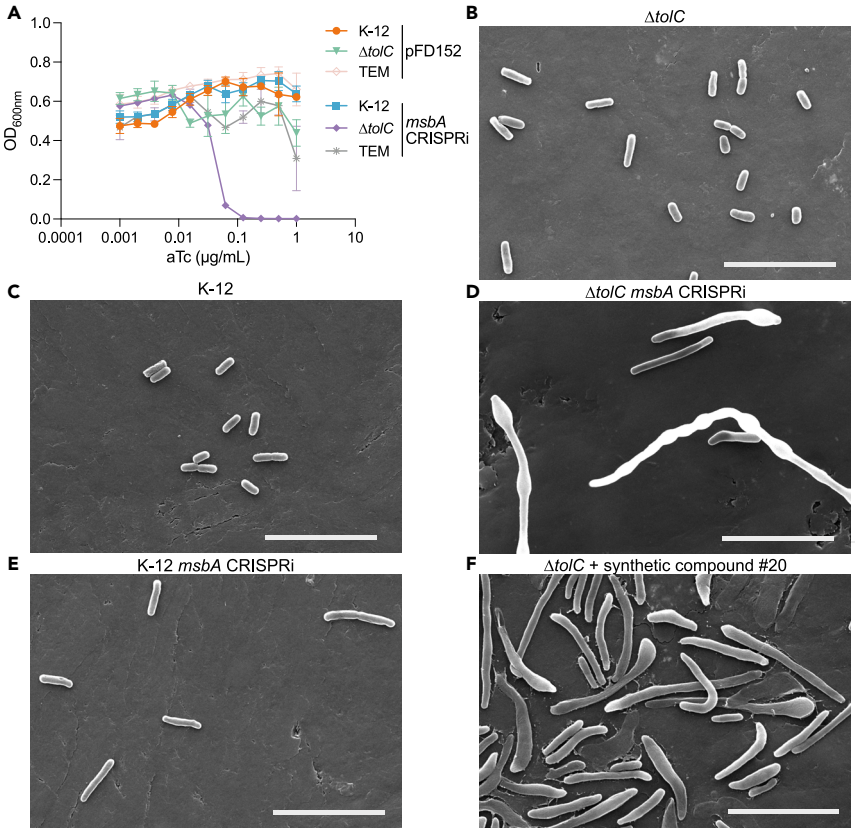

Figure 3. Identification of a synthetic-sick interaction between *tolC* and *msbA*

(A) CRISPRi-mediated *msbA* knockdown in the wild-type K-12, Δ*tolC*, and TE mutant strains propagated in the presence of increasing concentrations of the inducer anhydrotetracycline. The empty plasmid (pFD152) represents the negative control. Data points represent the average OD_{600nm} ± standard deviation of three technical replicates and are representative of three independent experiments.

(B–F) Scanning electron micrographs of (B) untreated Δ*tolC* and (C) K-12 during the mid-exponential growth phase. (D, E) CRISPRi-mediated repression of *msbA* (D) in Δ*tolC* and (E) K-12. (F) Chemical inhibition of MsbA in the presence of 0.5x the MIC of synthetic compound #20 in Δ*tolC*. Related to Figure S5. Scale bars represent 10 μm.

In summary, we have identified a distinct structural class of MsbA inhibitors that may exhibit different binding modes than previously described inhibitors.

Identification of a synthetic-sick interaction between *tolC* and *msbA*

Since the inactivation of *tolC* rendered *E. coli* hypersusceptible to two different classes of MsbA inhibitors (Figure 1), we hypothesized that a negative synthetic interaction existed between *tolC* and MsbA. Negative synthetic, or synthetic-sick, interactions refer to combinations of perturbations (e.g., either genetic or chemical) that induce a negative fitness defect different from the anticipated phenotype based on the effects of single perturbations.[28] As anticipated, CRISPRi-mediated knockdown of *msbA* revealed a synthetic-sick interaction between *msbA* and *tolC*, where the growth of the *tolC*-inactivated mutant was greatly reduced in response to *msbA* knockdown compared to the TE mutant and the wild-type strain (Figure 3A). Phenotypic analysis revealed that both the chemical inhibition of MsbA and the genetic repression of *msbA* induced severe morphological defects in Δ*tolC*, with filament formation, bulging, and tadpole-shaped defects emerging at the cell poles (Figures 3B–3F and S5). In summary, *tolC* inactivation sensitizes *E. coli* to both the chemical inhibition of MsbA and the genetic knockdown of *msbA*, identifying a synthetic-sick interaction.

TolC impacts the permeability and mechanical properties of the outer membrane

Based on the identified synthetic-sick interaction (Figure 3), we speculated that *tolC* inactivation could induce cell envelope defects that sensitize the strain to perturbations in LPS transport. As such, we investigated OM integrity by measuring the uptake of the fluorescent probe 1-*N*-phenylnaphthylamine (NPN).[29] This hydrophobic dye is ordinarily excluded by the OM, and disruption of the OM barrier function enables entry into the phospholipids, increasing fluorescence. Consistent with OM defects, NPN rapidly accumulated in the phospholipids of Δ*tolC* compared to the TE mutant (Figure 4A). We reasoned that the increase in OM permeability could explain the increased sensitivity of Δ*tolC* to the benzophenones

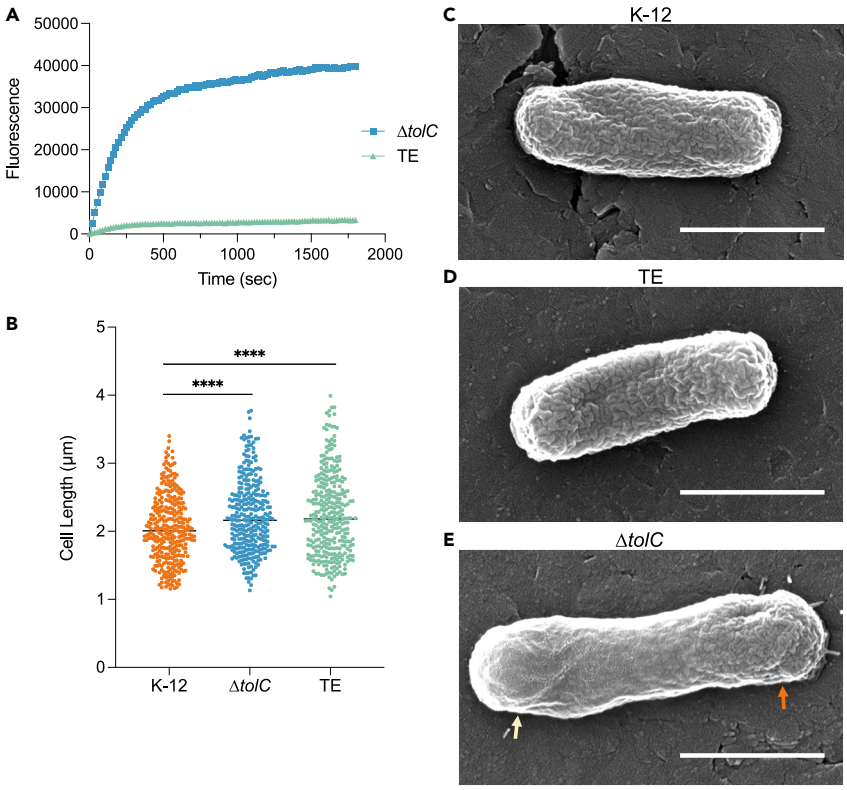

Figure 4. The inactivation of *tolC* reduces outer membrane integrity, impacting cell surface morphology

(A) NPN accumulation assays in the Δ*tolC* and TE mutants. Data points are background-subtracted averages of three technical replicates and are representative of two independent experiments.

(B) Cell length measurements of 325 cells from $n = 3$ biological replicates of scanning electron micrographs of the wild-type K-12, Δ*tolC*, and TE mutant strains. p values were calculated using a two-tailed Student's t test (****$p < 0.0001$, $p = 9.70 \times 10^{-6}$ and 4.50×10^{-6} for Δ*tolC* and the TE mutant, respectively).

(C–E) Scanning electron micrographs of (C) wild-type K-12, (D) the TE mutant, and (E) Δ*tolC* during the mid-exponential phase of growth. A subset of the Δ*tolC* cells displayed phenotypic heterogeneity, with regions of undulations and smoothness, which are indicated by the orange and yellow arrows, respectively. Images are representatives of three biological replicates. Scale bars represent 1 μm. Related to Figure S6.

compared to the TE mutant and the wild-type strain (Figure 1); however, we noted the susceptibility of the wild-type and TE mutant strains was not impacted by OM porination (Figure 1A; Table 1). To investigate further, we also profiled a *bamB*-inactivated mutant exhibiting a permeabilized OM[30] (Table 1) and wild-type cells treated with EDTA[31] (Figure S4D). Overall, increased OM permeability, as assessed using two different permeabilized strains and EDTA treatment, did not affect the sensitivity of *E. coli* K-12 (BW25113) to the benzophenones.

Next, the morphology of the Δ*tolC* mutant was characterized using scanning electron microscopy (SEM), revealing that the surfaces of Δ*tolC* cells were relatively "smoother" than the undulated cell surface of the wild-type and TE mutant strains (Figures 4C–4E and S6). Both efflux-deficient mutants were also moderately, yet significantly, longer compared to the wild-type cells (Figure 4B). Overall, it was not possible to statistically assess the extent of smoothness across the Δ*tolC* population since there was a high level of phenotypic heterogeneity across the cell population and even within a single bacterial cell (Figure 4E). However, we did not identify smooth phenotypes among the wild-type or TE mutant cells. While these phenotypic observations could be a consequence of the cell preparation method used for SEM, all strains were handled equally, revealing cell surface structural differences between the strains.

To further analyze the morphological structural changes between these strains in aqueous conditions, and to assess the contribution of TolC to cell envelope mechanics, single-cell atomic force microscopy (AFM)[32,33] was employed. High-resolution images of the cell surface revealed that the wild-type cells exhibited high-frequency undulations (Figures 5A, 5B, and S7), consistent with the SEM findings (Figure 4C). In contrast, Δ*tolC* cells appeared to be either very smooth or exhibited low-frequency undulations (Figures 5A, 5B, and S7). The TE mutant exhibited combinations of both characteristics (Figures 5A, 5B, and S7). The mean roughness values of the wild-type strain exhibited a much wider dispersion; however, these differences were not found to be significant (Figure S8B). Finally, we used AFM-based indentation experiments to quantify cell envelope mechanical properties, or OM stiffness (also called tensile elasticity).[34,35] The Young's modulus (E) and the spring constant (k) for the wild-type strain were consistent with previous studies[34,36,37] (Figures 5C–5F). Supporting the notion that Δ*tolC* exhibits a compromised OM, cell stiffness was shown to be significantly reduced in Δ*tolC* cells, with decreases in both E and k values (Figures 5C–5F and S9). In summary, our results show that *tolC* impacts the integrity and mechanical properties of the OM.

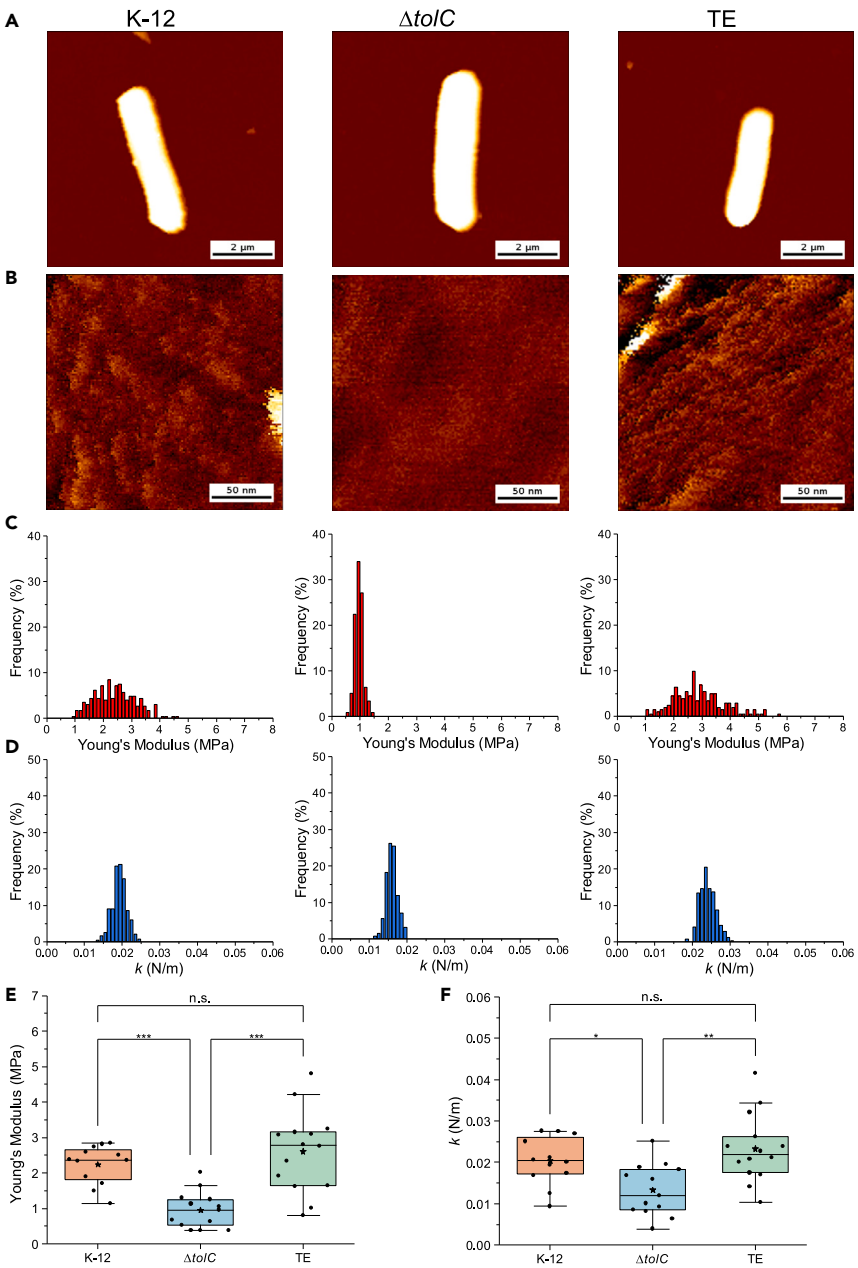

Figure 5. Inactivation of *tolC* impacts surface morphology and envelope mechanics of single live cells

(A) Representative low-resolution AFM height images of the wild-type K-12, Δ*tolC*, and TE mutant strains during the mid-exponential growth phase. Images were obtained in PBS, in quantitative imaging (QI) mode (8 μm × 8 μm, color scale: 800 nm).

(B) High-resolution height images. Images were obtained in QI mode (200 nm × 200 nm, color scale: 25 nm). Representative distributions of (C) Young's modulus and (D) spring constant (*k*) values obtained by AFM force–volume measurements in PBS across the surface of cells.

(E and F) Statistical analysis performed for each strain shows that *tolC*-inactivation significantly reduces cell envelope stiffness compared to the K-12 ($p = 9.13 \times 10^{-4}$ for Young's modulus and 3.92×10^{-2} for spring constant) and TE mutant strains ($p = 1.59 \times 10^{-5}$ for Young's modulus and 1.82×10^{-3} for spring constant). Boxplots show the individual (E) Young's modulus and (F) spring constant values obtained from $n = 12$ cells for K-12, $n = 13$ cells for Δ*tolC*, and $n = 14$ cells for the TE mutant. *p* values were calculated using Tukey's multiple comparison test (*$p \leq 0.05$, **$p \leq 0.01$, ***$p \leq 0.001$, n.s. = not significant). Shown are mean values (stars), 25% and 75% quartiles (boxes), medians (center line of boxes), and the standard deviation (whiskers). Related to Figures S7–S9.

DISCUSSION

The permeation and transport of compounds across the *E. coli* cell envelope is a complex phenomenon due to two membranes with orthogonal properties.[38] To facilitate the extrusion of toxic substances across the cell envelope, several IM efflux pumps complex with the OM channel TolC. In these instances, TolC essentially functions as a nonspecific passive conduit for expulsion across the OM. Supporting our previous findings,[9] we demonstrate that *tolC* inactivation affects antimicrobial susceptibility differently from the inactivation of genes encoding the IM efflux pumps that form complexes with TolC. Specifically, a *tolC* null strain was more sensitive to a panel of poorly characterized synthetic compounds than mutants lacking TolC-dependent IM pumps (Figure 1). While investigating the molecular basis of these susceptibility differences, we identified benzophenone-containing inhibitors that target the LPS transporter, MsbA.

MsbA is an essential ABC transporter responsible for translocating LPS to the outer leaflet of the IM; MsbA antagonism induces LPS accumulation at the cytoplasmic interface of the IM, causing perturbations in cellular ultrastructure.[14,15,39] MsbA is an integral membrane protein, forming a homodimer alternating between inward-facing and outward-facing conformations during transport.[40] Two different MsbA antagonist scaffolds have been identified: the quinoline series[18,19] and TBT-1.[17] Both classes bind the MsbA transmembrane region yet occupy adjacent and separate binding pockets.[22] Interestingly, TBT-1 stimulates ATPase activity and induces a collapsed inward-facing MsbA conformation, targeting the LPS substrate binding site.[22] The quinolines abolish ATPase hydrolysis,[18] interacting with the inward-facing MsbA conformation, preventing the closure of the protein by displacement of the nucleotide-binding domains.[22] In contrast, the benzophenones identified in this study appear to target a binding pocket localizing to the elbow helix of MsbA (Figure 1). One of the nonsynonymous mutations conferring high-level resistance to syn. #20 (Table 1) localizes to transmembrane helix 4 of MsbA ($R_{190}L$). In the occluded and outward-facing conformations, this amino acid comes into proximity with the proposed binding site (Figure 1), supporting a conformation-dependent binding site. However, we acknowledge that these mutations may not reside in the binding pocket and could instead affect the conformation of MsbA, reducing the drug's affinity. Nonetheless, despite the binding site remaining putative, the benzophenones demonstrated dose-dependent inhibition of MsbA, inducing LPS accumulation, and are structurally distinct from existing classes of MsbA inhibitors.

Notably, despite MsbA being considered essential for growth,[14,39] the benzophenones do not exhibit growth-inhibitory activity against wild-type *E. coli* strains (Table 1). We consequently revealed that intrinsic resistance mediated by the OM and active efflux does not appear to be responsible for the weak activity against wild-type *E. coli* strains. Indeed, the efflux-deficient TE and EKO-35 strains were insensitive to these inhibitors (Figure 1). Additionally, permeabilizing the OM, either through the introduction of a large nonspecific FhuA-derivatized pore,[10] through *bamB* inactivation, or using cells treated with EDTA, did not sensitize *E. coli* to the benzophenone-containing compound synthetic #20 (Table 1; Figure S4D). In contrast, antibacterial activity was observed in *E. coli* strains expressing the *imp4213* allele of *lptD*, which increases the abundance of phospholipids in the OM, increasing OM permeability.[20,41] However, the increased antibacterial activity may be the result of collateral damage due to disruptions in both MsbA-mediated LPS translocation and LptD/E-mediated LPS assembly at the cell surface.[42,43]

Compared to the quinolines, which are potent MsbA antagonists exhibiting low nM activity,[18,19] the benzophenones are relatively weak inhibitors (low μM activity) (Figure 2). We postulate that the level of MsbA antagonism provided by these inhibitors is not sufficient to inhibit growth in wild-type strains. Indeed, we also note that while CRISPRi-mediated knockdown of *msbA*—which reduced the *msbA* transcript levels by ~50% compared to the basal levels (Figure S2)—induced a lethal phenotype in Δ*tolC*, the growth of the wild-type strain remained largely unaffected (Figure 3A). Thus, we hypothesize that antagonists of MsbA must be potent (in the low nM range), or *msbA* transcript levels must be reduced >50%, to elicit growth inhibition. We subsequently hypothesized that the Δ*tolC* mutant exhibits a compromised OM, which sensitizes the strain to MsbA antagonism. Consequently, a synthetic-sick interaction was identified between *tolC* and *msbA* (Figures 1C and 3). The latter indicates that the susceptibility differences (Figure 1) observed between Δ*tolC* and the TE mutant are not merely a reflection of altered drug permeation.

Lipoproteins and LPS within the OM of *E. coli* confer stiffness and strength to the cell envelope.[44] As such, when the composition of the OM is altered, as exemplified by *E. coli* strains expressing the *imp4213* allele of *lptD*, OM stiffness is reduced.[44] Similarly, mutants lacking the abundant OM protein OmpA[44] and compromising the function of Braun's lipoprotein, Lpp, also decrease cell envelope stiffness, the latter of which is attributed to the protein's ability to link peptidoglycan to the OM, controlling the depth of the periplasm.[34,44] Consistent with the notion that *tolC* null mutants exhibit compromised cell envelopes, single-cell AFM revealed significant alteration in cell envelope mechanics, with reduced stiffness (Figure 5). Additionally, high-resolution SEM in conjunction with AFM height images revealed that the surface of Δ*tolC* cells is heterogeneous, with relatively "smooth" regions that were not observed in the wild-type or TE mutant strains (Figure 4). Taken together, our findings highlight that disruptions in *tolC* impact the integrity of the cell envelope, which we believe sensitizes *E. coli* to perturbations in LPS transport.

Several factors could underlie this phenomenon. TolC is intricately associated with Enterobacteriaceae physiology, being implicated in the export of potentially toxic metabolites that could accumulate, inducing membrane damage.[8,11,45,46] Indeed, enterobactin accumulation under iron-limited conditions in *tolC* null mutants leads to a metabolic shutdown, cell envelope stress, and severe growth defects.[8,11,45,46] Cell envelope stress and loss of integrity could underlie the increased sensitivity of Δ*tolC*; however, our phenotypes are evident in iron-replete, optimal growth conditions. Additionally, metabolite extrusion is associated with the efflux pumps absent in the TE mutant, and the mechanics of the cell envelope in the TE mutant are comparable to that of the wild-type strain (Figure 5). An alternative hypothesis is that *tolC* inactivation disrupts OM asymmetry and composition; TolC mutants exhibit decreases in the abundance of the OmpF and OmpC porins, whereas the OmpA abundance is only slightly reduced.[47] OmpF and OmpC interact with the OM lipoprotein MlaA, a component of the Mla system,

preventing phospholipid accumulation in the outer leaflet of the OM and maintaining asymmetry.[48] As such, reductions in OmpC and OmpF could interfere with the Mla system. Overall, the role of TolC in the physiology of *E. coli* under iron-replete and optimal growth conditions remains to be established and will be the focus of future studies.

In summary, our findings reveal that *tolC* inactivation impacts cell envelope integrity, reduces OM stiffness, and sensitizes *E. coli* to perturbations in LPS transport. Additionally, we report the identification of a distinct class of inhibitors targeting MsbA, which could be optimized to improve activity against wild-type *E. coli* and could also be used as probes to study the function of MsbA since they target a region of the protein distinct from other known inhibitors. Interestingly, the identified synthetic-sick interaction appears distinct from TolC-associated drug-effluxing activities. Such an observation, in combination with the cell envelope defects induced by loss of *tolC*, suggests that these factors should be considered when using *tolC* null strains to study efflux deficiency. Finally, our findings reveal that the susceptibility differences observed between *tolC* null mutants and the efflux-deficient EKO-35 and TE mutant strains could be exploited to identify new inhibitors of cell envelope biogenesis. Indeed, in addition to syn #20, we have identified several synthetic compounds that exhibit increased activity against the *tolC* null mutant (Figure 1). Preliminary studies revealed *msbA* overexpression did not impact the susceptibility of Δ*tolC* to these compounds (Figure S10), indicating that MsbA may not be the target. We speculate that these inhibitors could target other components of the cell envelope biosynthesis machinery and that further *tolC*-associated synthetic interactions exist, which will be the focus of future studies.

Limitations of the study

The mechanistic work described in this study was mostly undertaken in *E. coli* K-12; future studies should ascertain whether our findings are also observed in other strains of *E. coli*.

STAR★METHODS

Detailed methods are provided in the online version of this paper and include the following:

- KEY RESOURCES TABLE
- RESOURCE AVAILABILITY
  - Lead contact
  - Materials availability
  - Data and code availability
- EXPERIMENTAL MODEL AND STUDY PARTICIPANT DETAILS
  - Strains, plasmids, and growth conditions
- METHOD DETAILS
  - Generation of the TE mutant
  - Whole genome sequencing of Δ*tolC* and the TE mutant
  - Generation of synthetic #20 resistant mutants
  - Antimicrobial susceptibility testing
  - RT-qPCR
  - CRISPRi-mediated *msbA* repression
  - MsbA ATPase assay
  - Thin-section transmission electron microscopy
  - Outer membrane permeability assay
  - Scanning electron microscopy
  - Atomic force microscopy
- QUANTIFICATION AND STATISTICAL ANALYSIS

SUPPLEMENTAL INFORMATION

Supplemental information can be found online at https://doi.org/10.1016/j.isci.2024.109592.

ACKNOWLEDGMENTS

This work was supported by a Natural Sciences and Engineering Research Council of Canada (NSERC) Discovery grant (no. RGPIN-2019-04996) and a Canada Foundation for Innovation (CFI) grant no. JELF 37730 awarded to G.C., an Ontario Graduate Scholarship and Canadian Graduate Scholarship awarded to S.Z., and an Ontario Graduate Scholarship awarded to K.R. This study was also supported by a Foundation grant from the Canadian Institutes of Health Research (grant no. FRN 143215), infrastructure funding from the CFI, a Research Excellence allocation from the Ontario Research Fund, and a Tier I Canada Research Chair award to E.D.B. Work at UCLouvain was supported by the National Fund for Scientific Research (FNRS). We thank Dr. S.D. Kelly (Whitfield laboratory, University of Guelph) for providing the *E. coli* TUC01 strain used for the *cat-sacB* cassette amplification. We also thank J.A. Goetz and S.E. Gilbert for assistance in generating the TE mutant strain and L.K. Thompson for assistance with analysis of the TE mutant genome. Lastly, we thank Drs. E. Roach and E. Anderson (Molecular and Cellular Imaging Facility, University of Guelph) for technical assistance obtaining scanning electron microscopy images.

AUTHOR CONTRIBUTIONS

G.C. conceived the research, and G.C., M.K.A., V.V., E.D.B., and Y.F.D. guided the research. G.C., S.Z., M.K.A., T.O.P., K.R., A.M., Y.X., V.V., M.R., Y.F.D., and E.D.B. designed the experiments. S.Z., M.K.A., T.O.P., K.R., A.M., Y.X., V.V., and M.R. performed the experiments and analyzed the data. G.C. and S.Z. wrote the manuscript and all authors commented on and approved the paper.

DECLARATION OF INTERESTS

The authors declare no competing interests.

Received: December 1, 2023
Revised: February 2, 2024
Accepted: March 25, 2024
Published: March 27, 2024

REFERENCES

1. Guest, R.L., and Silhavy, T.J. (2023). Cracking outer membrane biogenesis. Biochim. Biophys. Acta. Mol. Cell Res. *1870*, 119405.
2. Cox, G., and Wright, G.D. (2013). Intrinsic antibiotic resistance: mechanisms, origins, challenges and solutions. Int. J. Med. Microbiol. *303*, 287–292.
3. Zgurskaya, H.I., and Rybenkov, V.V. (2020). Permeability barriers of Gram-negative pathogens. Ann. N. Y. Acad. Sci. *1459*, 5–18.
4. Benn, G., Mikheyeva, I.V., Inns, P.G., Forster, J.C., Ojkic, N., Bortolini, C., Ryadnov, M.G., Kleanthous, C., Silhavy, T.J., and Hoogenboom, B.W. (2021). Phase separation in the outer membrane of *Escherichia coli*. Proc. Natl. Acad. Sci. USA *118*, e2112237118. https://doi.org/10.1073/pnas.2112237118.
5. Sun, J., Rutherford, S.T., Silhavy, T.J., and Huang, K.C. (2022). Physical properties of the bacterial outer membrane. Nat. Rev. Microbiol. *20*, 236–248.
6. Fivenson, E.M., Rohs, P.D.A., Vettiger, A., Sardis, M.F., Torres, G., Forchoh, A., and Bernhardt, T.G. (2023). A role for the Gram-negative outer membrane in bacterial shape determination. Proc. Natl. Acad. Sci. USA *120*, e2301987120.
7. Krishnamoorthy, G., Leus, I.V., Weeks, J.W., Wolloscheck, D., Rybenkov, V.V., and Zgurskaya, H.I. (2017). Synergy between Active Efflux and Outer Membrane Diffusion Defines Rules of Antibiotic Permeation into Gram-Negative Bacteria. mBio *8*, e01172-17. https://doi.org/10.1128/mBio.01172-17.
8. Teelucksingh, T., Thompson, L.K., and Cox, G. (2020). The Evolutionary Conservation of *Escherichia coli* Drug Efflux Pumps Supports Physiological Functions. J. Bacteriol. *202*, e00367-20. https://doi.org/10.1128/JB.00367-20.
9. Teelucksingh, T., Thompson, L.K., Zhu, S., Kuehfuss, N.M., Goetz, J.A., Gilbert, S.E., MacNair, C.R., Geddes-McAlister, J., Brown, E.D., and Cox, G. (2022). A genetic platform to investigate the functions of bacterial drug efflux pumps. Nat. Chem. Biol. *18*, 1399–1409. https://doi.org/10.1038/s41589-022-01119-y.
10. Krishnamoorthy, G., Wolloscheck, D., Weeks, J.W., Croft, C., Rybenkov, V.V., and Zgurskaya, H.I. (2016). Breaking the Permeability Barrier of *Escherichia coli* by Controlled Hyperporination of the Outer Membrane. Antimicrob. Agents Chemother. *60*, 7372–7381.
11. Zgurskaya, H.I., Krishnamoorthy, G., Ntreh, A., and Lu, S. (2011). Mechanism and Function of the Outer Membrane Channel TolC in Multidrug Resistance and Physiology of Enterobacteria. Front. Microbiol. *2*, 189.
12. Baba, T., Ara, T., Hasegawa, M., Takai, Y., Okumura, Y., Baba, M., Datsenko, K.A., Tomita, M., Wanner, B.L., and Mori, H. (2006). Construction of *Escherichia coli* K-12 in-frame, single-gene knockout mutants: the Keio collection. Mol. Syst. Biol. *2*, 2006.0008.
13. El Zahed, S.S., French, S., Farha, M.A., Kumar, G., and Brown, E.D. (2021). Physicochemical and Structural Parameters Contributing to the Antibacterial Activity and Efflux Susceptibility of Small Molecule Inhibitors of *Escherichia coli*. Antimicrob. Agents Chemother. *65*, e01925-20. https://doi.org/10.1128/AAC.01925-20.
14. Doerrler, W.T., Reedy, M.C., and Raetz, C.R. (2001). An *Escherichia coli* mutant defective in lipid export. J. Biol. Chem. *276*, 11461–11464.
15. Voss, B.J., and Trent, M.S. (2018). LPS Transport: Flipping Out over MsbA. Curr. Biol. *28*, R30–R33.
16. Guo, D., Singh, H., Shimoyama, A., Guffick, C., Tang, Y., Rowe, S.M., Noel, T., Spring, D.R., Fukase, K., and van Veen, H.W. (2021). Energetics of lipid transport by the ABC transporter MsbA is lipid dependent. Commun. Biol. *4*, 1379.
17. Zhang, G., Baidin, V., Pahil, K.S., Moison, E., Tomasek, D., Ramadoss, N.S., Chatterjee, A.K., McNamara, C.W., Young, T.S., Schultz, P.G., et al. (2018). Cell-based screen for discovering lipopolysaccharide biogenesis inhibitors. Proc. Natl. Acad. Sci. USA *115*, 6834–6839.
18. Ho, H., Miu, A., Alexander, M.K., Garcia, N.K., Oh, A., Zilberleyb, I., Reichelt, M., Austin, C.D., Tam, C., Shriver, S., et al. (2018). Structural basis for dual-mode inhibition of the ABC transporter MsbA. Nature *557*, 196–201.
19. Alexander, M.K., Miu, A., Oh, A., Reichelt, M., Ho, H., Chalouni, C., Labadie, S., Wang, L., Liang, J., Nickerson, N.N., et al. (2018). Disrupting Gram-Negative Bacterial Outer Membrane Biosynthesis through Inhibition of the Lipopolysaccharide Transporter MsbA. Antimicrob. Agents Chemother. *62*, e01142-18. https://doi.org/10.1128/AAC.01142-18.
20. Ruiz, N., Falcone, B., Kahne, D., and Silhavy, T.J. (2005). Chemical Conditionality: A GeneticStrategy to Probe Organelle Assembly. Cell *121*, 307–317.
21. Verma, V.A., Wang, L., Labadie, S.S., Liang, J., Sellers, B.D., Wang, J., Dong, L., Wang, Q., Zhang, S., Xu, Z., et al. (2022). Discovery of Inhibitors of the Lipopolysaccharide Transporter MsbA: From a Screening Hit to Potent Wild-Type Gram-Negative Activity. J. Med. Chem. *65*, 4085–4120.
22. Thélot, F.A., Zhang, W., Song, K., Xu, C., Huang, J., and Liao, M. (2021). Distinct allosteric mechanisms of first-generation MsbA inhibitors. Science *374*, 580–585.
23. Smriti, Zou, P., Zou, P., and Mchaourab, H.S. (2009). Mapping daunorubicin-binding Sites in the ATP-binding cassette transporter MsbA using site-specific quenching by spin labels. J. Biol. Chem. *284*, 13904–13913.
24. Lyu, J., Liu, C., Zhang, T., Schrecke, S., Elam, N.P., Packianathan, C., Hochberg, G.K.A., Russell, D., Zhao, M., and Laganowsky, A. (2022). Structural basis for lipid and copper regulation of the ABC transporter MsbA. Nat. Commun. *13*, 7291.
25. Eckford, P.D.W., and Sharom, F.J. (2008). Functional characterization of *Escherichia coli* MsbA: interaction with nucleotides and substrates. J. Biol. Chem. *283*, 12840–12850.
26. Siarheyeva, A., and Sharom, F.J. (2009). The ABC transporter MsbA interacts with lipid A and amphipathic drugs at different sites. Biochem. J. *419*, 317–328.
27. Woebking, B., Reuter, G., Shilling, R.A., Velamakanni, S., Shahi, S., Venter, H., Balakrishnan, L., and van Veen, H.W. (2005). Drug-lipid A interactions on the *Escherichia coli* ABC transporter MsbA. J. Bacteriol. *187*, 6363–6369.
28. Klobucar, K., and Brown, E.D. (2018). Use of genetic and chemical synthetic lethality as probes of complexity in bacterial cell systems. FEMS Microbiol. Rev. *42*, 81–99. https://doi.org/10.1093/femsre/fux054.
29. Helander, I.M., and Mattila-Sandholm, T. (2000). Fluorometric assessment of gram-negative bacterial permeabilization. J. Appl. Microbiol. *88*, 213–219.
30. King, A.M., Reid-Yu, S.A., Wang, W., King, D.T., De Pascale, G., Strynadka, N.C., Walsh, T.R., Coombes, B.K., and Wright, G.D. (2014). Aspergillomarasmine A overcomes metallo-β-lactamase antibiotic resistance. Nature *510*, 503–506.
31. Vaara, M. (1992). Agents that increase the permeability of the outer membrane. Microbiol. Rev. *56*, 395–411.
32. Dufrêne, Y.F., Ando, T., Garcia, R., Alsteens, D., Martinez-Martin, D., Engel, A., Gerber, C., and Müller, D.J. (2017). Imaging modes of atomic force microscopy for application in molecular and cell biology. Nat. Nanotechnol. *12*, 295–307.

33. Viljoen, A., Mathelié-Guinlet, M., Ray, A., Strohmeyer, N., Oh, Y.J., Hinterdorfer, P., Müller, D.J., Alsteens, D., and Dufrêne, Y.F. (2021). Force spectroscopy of single cells using atomic force microscopy. Nat. Rev. Methods Primers *1*, 63.
34. Mathelié-Guinlet, M., Asmar, A.T., Collet, J.-F., and Dufrêne, Y.F. (2020). Lipoprotein Lpp regulates the mechanical properties of the *E. coli* cell envelope. Nat. Commun. *11*, 1789.
35. Krieg, M., Fläschner, G., Alsteens, D., Gaub, B.M., Roos, W.H., Wuite, G.J.L., Gaub, H.E., Gerber, C., Dufrêne, Y.F., and Müller, D.J. (2018). Atomic force microscopy-based mechanobiology. Nat. Rev. Phys. *1*, 41–57.
36. Mathelié-Guinlet, M., Grauby-Heywang, C., Martin, A., Février, H., Moroté, F., Vilquin, A., Béven, L., Delville, M.-H., and Cohen-Bouhacina, T. (2018). Detrimental impact of silica nanoparticles on the nanomechanical properties of *Escherichia coli*, studied by AFM. J. Colloid Interface Sci. *529*, 53–64.
37. Longo, G., Rio, L.M., Roduit, C., Trampuz, A., Bizzini, A., Dietler, G., and Kasas, S. (2012). Force volume and stiffness tomography investigation on the dynamics of stiff material under bacterial membranes. J. Mol. Recognit. *25*, 278–284.
38. Silver, L.L. (2016). A Gestalt approach to Gram-negative entry. Bioorg. Med. Chem. *24*, 6379–6389.
39. Zhou, Z., White, K.A., Polissi, A., Georgopoulos, C., and Raetz, C.R. (1998). Function of *Escherichia coli* MsbA, an essential ABC family transporter, in lipid A and phospholipid biosynthesis. J. Biol. Chem. *273*, 12466–12475.
40. Mi, W., Li, Y., Yoon, S.H., Ernst, R.K., Walz, T., and Liao, M. (2017). Structural basis of MsbA-mediated lipopolysaccharide transport. Nature *549*, 233–237.
41. Sampson, B.A., Misra, R., and Benson, S.A. (1989). Identification and characterization of a new gene of *Escherichia coli* K-12 involved in outer membrane permeability. Genetics *122*, 491–501.
42. Braun, M., and Silhavy, T.J. (2002). Imp/OstA is required for cell envelope biogenesis in *Escherichia coli*. Mol. Microbiol. *45*, 1289–1302.
43. Wu, T., McCandlish, A.C., Gronenberg, L.S., Chng, S.-S., Silhavy, T.J., and Kahne, D. (2006). Identification of a protein complex that assembles lipopolysaccharide in the outer membrane of *Escherichia coli*. Proc. Natl. Acad. Sci. USA *103*, 11754–11759.
44. Rojas, E.R., Billings, G., Odermatt, P.D., Auer, G.K., Zhu, L., Miguel, A., Chang, F., Weibel, D.B., Theriot, J.A., and Huang, K.C. (2018). The outer membrane is an essential load-bearing element in Gram-negative bacteria. Nature *559*, 617–621.
45. Guest, R.L., Court, E.A., Waldon, J.L., Schock, K.A., and Raivio, T.L. (2019). Impaired Efflux of the Siderophore Enterobactin Induces Envelope Stress in *Escherichia coli*. Front. Microbiol. *10*, 2776.
46. Bleuel, C., Grosse, C., Taudte, N., Scherer, J., Wesenberg, D., Krauss, G.J., Nies, D.H., and Grass, G. (2005). TolC is involved in enterobactin efflux across the outer membrane of *Escherichia coli*. J. Bacteriol. *187*, 6701–6707.
47. Morona, R., and Reeves, P. (1982). The tolC locus of *Escherichia coli* affects the expression of three major outer membrane proteins. J. Bacteriol. *150*, 1016–1023.
48. Chong, Z.-S., Woo, W.-F., and Chng, S.-S. (2015). Osmoporin OmpC forms a complex with MlaA to maintain outer membrane lipid asymmetry in *Escherichia coli*. Mol. Microbiol. *98*, 1133–1146.
49. Thomason, L.C., Sawitzke, J.A., Li, X., Costantino, N., and Court, D.L. (2014). Recombineering: genetic engineering in bacteria using homologous recombination. Curr. Protoc. Mol. Biol. *106*, 1.16.1–1.16.39.
50. Grenier, F., Matteau, D., Baby, V., and Rodrigue, S. (2014). Complete Genome Sequence of *Escherichia coli* BW25113. Genome Announc. *2*, e01038-14. https://doi.org/10.1128/genomea.01038-14.
51. Kehlenbeck, D.-M., Traore, D.A.K., Josts, I., Sander, S., Moulin, M., Haertlein, M., Prevost, S., Forsyth, V.T., and Tidow, H. (2022). Cryo-EM structure of MsbA in saposin-lipid nanoparticles (Salipro) provides insights into nucleotide coordination. FEBS J. *289*, 2959–2970.
52. Ward, A., Reyes, C.L., Yu, J., Roth, C.B., and Chang, G. (2007). Flexibility in the ABC transporter MsbA: Alternating access with a twist. Proc. Natl. Acad. Sci. USA *104*, 19005–19010.
53. Datsenko, K.A., and Wanner, B.L. (2000). One-step inactivation of chromosomal genes in *Escherichia coli* K-12 using PCR products. Proc. Natl. Acad. Sci. USA *97*, 6640–6645.
54. Jiang, Y., Chen, B., Duan, C., Sun, B., Yang, J., and Yang, S. (2015). Multigene editing in the *Escherichia coli* genome via the CRISPR-Cas9 system. Appl. Environ. Microbiol. *81*, 2506–2514.
55. Depardieu, F., and Bikard, D. (2020). Gene silencing with CRISPRi in bacteria and optimization of dCas9 expression levels. Methods *172*, 61–75.
56. Rachwalski, K., Tu, M.M., Madden, S.J., French, S., Hansen, D.M., and Brown, E.D. (2024). A mobile CRISPRi collection enables genetic interaction studies for the essential genes of *Escherichia coli*. Cell Rep. Methods *4*, 100693.
57. Cox, G., Sieron, A., King, A.M., De Pascale, G., Pawlowski, A.C., Koteva, K., and Wright, G.D. (2017). A Common Platform for Antibiotic Dereplication and Adjuvant Discovery. Cell Chem. Biol. *24*, 98–109.
58. Schindelin, J., Arganda-Carreras, I., Frise, E., Kaynig, V., Longair, M., Pietzsch, T., Preibisch, S., Rueden, C., Saalfeld, S., Schmid, B., et al. (2012). Fiji: an open-source platform for biological-image analysis. Nat. Methods *9*, 676–682.
59. Kolmogorov, M., Yuan, J., Lin, Y., and Pevzner, P.A. (2019). Assembly of long, error-prone reads using repeat graphs. Nat. Biotechnol. *37*, 540–546.
60. Kearse, M., Moir, R., Wilson, A., Stones-Havas, S., Cheung, M., Sturrock, S., Buxton, S., Cooper, A., Markowitz, S., Duran, C., et al. (2012). Geneious Basic: an integrated and extendable desktop software platform for the organization and analysis of sequence data. Bioinformatics *28*, 1647–1649.
61. Deatherage, D.E., and Barrick, J.E. (2014). Identification of mutations in laboratory-evolved microbes from next-generation sequencing data using breseq. Methods Mol. Biol. *1151*, 165–188.
62. Wistrand-Yuen, E., Knopp, M., Hjort, K., Koskiniemi, S., Berg, O.G., and Andersson, D.I. (2018). Evolution of high-level resistance during low-level antibiotic exposure. Nat. Commun. *9*, 1599.
63. Patel, J.B., Cockerill, F.R., Bradford, A.P., Eliopoulos, M.G., Hindler, A.J., Jenkins, G.S., Lewis, S.J., Limbago, B., Miller, A.L., Nicolau, P.D., et al. (2015). M07-A10: Methods for Dilution Antimicrobial Susceptibility Tests for Bacteria that Grow Aerobically; Approved Standard—Tenth Edition (CLSI (Clinical Lab Stand Institute)).
64. Bustin, S.A., Benes, V., Garson, J.A., Hellemans, J., Huggett, J., Kubista, M., Mueller, R., Nolan, T., Pfaffl, M.W., Shipley, G.L., et al. (2009). The MIQE guidelines: minimum information for publication of quantitative real-time PCR experiments. Clin. Chem. *55*, 611–622.
65. Rocha, D.J.P., Santos, C.S., and Pacheco, L.G.C. (2015). Bacterial reference genes for gene expression studies by RT-qPCR: survey and analysis. Antonie Leeuwenhoek *108*, 685–693.
66. Livak, K.J., and Schmittgen, T.D. (2001). Analysis of relative gene expression data using real-time quantitative PCR and the 2(-Delta Delta C(T)) Method. Methods *25*, 402–408.
67. Sader, J.E., Larson, I., Mulvaney, P., and White, L.R. (1995). Method for the calibration of atomic force microscope cantilevers. Rev. Sci. Instrum. *66*, 3789–3798.
68. Thomas, G., Burnham, N.A., Camesano, T.A., and Wen, Q. (2013). Measuring the mechanical properties of living cells using atomic force microscopy. J. Vis. Exp. *76*, 50497. https://doi.org/10.3791/50497.

STAR★METHODS

KEY RESOURCES TABLE

REAGENT or RESOURCE	SOURCE	IDENTIFIER
Bacterial and virus strains		
E. coli K-12 str. BW25113	Baba et al.[12]	N/A
E. coli CFT073	ATCC	ATCC 700928
E. coli CFT073 *lptD(imp4213)*	Ho et al.[18]	N/A
E. coli EKO-35	Teelucksingh & Thompson et al.[9]	N/A
E. coli pore	Teelucksingh & Thompson et al.[9]	N/A
E. coli TE mutant	This paper	N/A
E. coli Δ*tolC*	Baba et al.[12]	N/A
E. coli Δ*bamB*	Baba et al.[12]	N/A
E. coli TUC01	Thomason et al.[49]	N/A
Chemicals, peptides, and recombinant proteins		
Ampicillin	Bioshop	Cat# AMP201
Kanamycin	Bioshop	Cat# KAN201
Spectinomycin	Bioshop	Cat# SPE201
Chloramphenicol	Sigma-Aldrich	Cat# C0378
Anhydrotetracycline	Sigma-Aldrich	Cat# J66688.MA
Synthetic compound #20	Fisher Thermo Scientific	Cat# RH01772SC
G332	Genentech	N/A
G913	Genentech	N/A
G662	Genentech	N/A
G717	Genentech	N/A
G511	Genentech	N/A
G615	Genentech	N/A
Diaminopimelic acid (DAP)	Sigma-Aldrich	Cat# D1377
Gentamicin	BioBasic	Cat# GB0217
Vancomycin	Bioshop	Cat# VAN990
1-*N*-phenylnaphthylamine (NPN)	Sigma-Aldrich	Cat# 104043
Carbonyl cyanide *m*-chlorophenyl hydrazone (CCCP)	Sigma-Aldrich	Cat# C2759
Bovine serum albumin	HyClone™	Cat# SH3057402
Critical commercial assays		
2× GB-AMP™ PaCeR™ polymerase master mix	GeneBio Systems	Cat# PCR-002-01
Taq 2× polymerase master mix	FroggaBio	Cat# FBTAQM
GeneJET PCR purification kit	Thermo Fisher Scientific	Cat# K0701
GeneJET Plasmid Miniprep kit	Thermo Fisher Scientific	Cat# K0502
PureLink™ Genomic DNA Mini Kit	Invitrogen	Cat# K182001
RNeasy Mini Kit	Qiagen	Cat# 74104
TURBO DNA-Free Kit	Invitrogen	Cat# AM1907
Superscript™ IV First Strand Synthesis System Kit	Invitrogen	Cat# 18091050
Powertrack SYBR Green Master Mix kit	Thermo Fisher Scientific	Cat# A46012
Transcreener ADP2 FP Assay	BellBrook Labs	Cat# 3010

(*Continued on next page*)

Continued

REAGENT or RESOURCE	SOURCE	IDENTIFIER
Deposited data		
Raw whole genome sequencing data	This paper	BioProject ID PRJNA990483
E. coli K-12 str. BW25113 genome	Grenier et al.[50]	Accession no. CP009273.1
Inward-facing MsbA	Verma et al.[21]	PDB 7SEL
Occluded MsbA	Kehlenbeck et al.[51]	PDB 7BCW
Outward-facing MsbA	Ward et al.[52]	PDB 3B60
Oligonucleotides		
Primers used in this work	This paper	See Table S5
Recombinant DNA		
pKD46	Datsenko and Wanner.[53]	N/A
pCP20	Datsenko and Wanner.[53]	N/A
pCas	Jiang et al.[54]	Addgene Cat#62225
pTargetF	Jiang et al.[54]	Addgene Cat#62226
pFD152	Depardieu and Bikard.[55,56]	N/A
pGDP2	Cox et al.[57]	N/A
Software and algorithms		
Prism 9.4.1	GraphPad	https://www.graphpad.com/
ImageJ (Fiji)	Schindelin et al.[58]	https://imagej.net/software/fiji/
Benchling	Benchling	https://www.benchling.com/
Excel 16.36	Microsoft	https://www.office.com/
Geneious Prime v2020.2.4	Dotmatics	https://www.geneious.com/
Flye *de novo* assembler	Kolmogorov et al.[59]	https://github.com/fenderglass/Flye
QuantiGene Plex Data Analysis Version 2.6.2	Thermo Fisher	https://apps.thermofisher.com/apps/quantigene
OriginPro 2021	Origin Lab	https://www.originlab.com/
Other		
SeqCenter	SeqCenter	N/A
University of Guelph Advanced Analysis Center, Molecular and Cellular Imaging Facility – FEI Quanta FEG 250	Elecmi	N/A
QuantStudio 3 Real-Time PCR System	Applied Biosystems	Cat# A28567
BioTek Synergy H1 microplate reader	Agilent	N/A
JPK NanoWizard® 4 NanoScience	Bruker	N/A

RESOURCE AVAILABILITY

Lead contact

Further inquiries and requests should be directed to the lead contact, Dr. Georgina Cox (gcox@uoguelph.ca).

Materials availability

Reagents and bacteria used for the biological studies were obtained from the commercial or internal sources listed in the key resources table. The TE mutant strain generated in this study can be obtained from the lead contact.

Data and code availability

- The raw genomic sequencing data of Δ*tolC* and the TE mutant (before and after the repair of non-synonymous mutations) were deposited in GenBank (BioProject ID PRJNA990483). All further data reported in this paper can be shared by the lead contact upon request.
- The MsbA crystal structures used in this study were obtained from the Protein DataBank (PDB 7SEL; PDB 7BCW; PDB 3B60).
- The *E. coli* BW25113 genome sequence was obtained from GenBank (Accession no. CP009273.1).

- This paper does not report original code.
- Any additional information required to reanalyze the data reported in this paper is available from the lead contact upon request.

EXPERIMENTAL MODEL AND STUDY PARTICIPANT DETAILS

Strains, plasmids, and growth conditions

Bacterial strains and plasmids used in this study are provided in the key resources table and Table S4. *E. coli* K-12 str. BW25113[12,50] and the uropathogenic *E. coli* CFT073 were used as wild-type strains in this study. The *E. coli* TOP10 and DH5α strains were used as routine cloning hosts. The Δ*tolC* mutant and strains for resistance cassette amplification were obtained from the Keio Collection.[12] Plasmids for CRISPR–Cas9-mediated counter selection, pCas, and pTargetF, were purchased from Addgene.[54] Plasmids for the λ-Red recombinase system, pKD46 and pCP20,[53] and the constitutive expression of genes, pGDP-2,[57] were used as previously described. The kanamycin-resistance cassette from Δ*tolC* was removed using pCP20, the genome of this strain was then sequenced, and the strain was used for all aspects of this study. For the knockdown of *msbA*, sgRNA targeting *msbA* in *E. coli* was ligated into the conjugative CRISPRi plasmid, pFD152, using a previously described single-step golden gate assembly protocol.[55,56]

Strains were routinely propagated in Lysogeny broth (LB) (Bioshop) at 37°C or 30°C with aeration (220 r.p.m.). When grown in microtiter plates, strains were aerated at 900 r.p.m. For the selection of resistance markers, ampicillin (100 μg/mL) (Bioshop), kanamycin (50 μg/mL) (Sigma-Aldrich), spectinomycin (150 μg/mL) (Bioshop), and chloramphenicol (15 μg/mL) (Bioshop) were used at the listed concentrations. Susceptibility testing was conducted in cation-adjusted Mueller Hinton II Broth (MHB II) (BD Difco).

METHOD DETAILS

Generation of the TE mutant

The TE mutant was generated using λ-Red recombination[53] and CRISPR–Cas9-mediated counter selection.[54] Eight efflux genes were inactivated in the order shown in Table S1. Nucleic acid amplification was achieved using the high-fidelity 2× GB-AMP PaCeR polymerase master mix (GeneBio Systems Inc) or the Taq 2× polymerase master mix (FroggaBio) according to the manufacturers' guidelines. Amplicons were purified using the GeneJET PCR purification kit (Thermo Fisher Scientific) and plasmids were extracted and purified from saturated cultures using the GeneJET Plasmid Miniprep kit (Thermo Fisher Scientific) according to the manufacturer's suggested guidelines.

For λ-Red recombineering, the pKD46 plasmid was transformed into recipient strains using electroporation.[53] Broth cultures were grown to the mid-exponential phase of growth (OD_{600nm}–0.5) in the presence of ampicillin and 4 mM arabinose. The genes of interest were replaced with kanamycin-resistance cassettes from the appropriate Keio strain, which were amplified using PaCeR and primers annealing 50 bp upstream and downstream of the desired region (Table S5). To disrupt the genes of interest, recombinase-induced electrocompetent cells were transformed with 500 ng of purified amplicons. Strains harboring successful gene deletions were transformed with pCP20 to excise the resistance cassette.

For CRISPR-Cas9-mediated counterselection, the methodology described by Jiang et al.[54] was modified as previously described.[9] CRISPR guide software (Benchling) was used for the selection of sgRNA (N20) sequences, which were introduced into pTargetF by PCR (Table S5). Single-stranded DNA repair oligonucleotides were designed to introduce three tandem stop codons, a silent mutation to remove the PAM, and a silent mutation to introduce an *Ase*I restriction enzyme site for screening of successful mutants. Electrocompetent cells were transformed with 50 ng of pCas. A 50 mL broth culture was grown at 30°C to an OD_{600nm} of 0.5 in the presence of kanamycin and 4 mM arabinose for recombinase induction. Recombinase-induced electrocompetent cells were then transformed with 100 ng of pTargetF modified with a sgRNA and 2000 ng of ssDNA repair oligonucleotide. The cells were recovered in 1 mL of LB at 30°C, then grown overnight on LB agar supplemented with kanamycin and spectinomycin. Amplicons were then digested with the *Ase*I restriction enzyme (FastDigest enzyme series, Thermo Fisher Scientific) to screen for successful mutants. Gene disruptions were confirmed using Sanger sequencing (The Center for Applied Genomics, SickKids or Advanced Analysis Center, University of Guelph).

Four secondary mutations were identified in the TE mutant's genome (Table S1), including non-synonymous mutations in *hdfR, yjfC,* and *pitA*. CRISPR-Cas9-mediated counterselection was used to repair the mutations in *hdfR* and *yjfC*, which introduced two intentional silent mutations to remove the adjacent PAM site and for restriction enzyme-guided screening purposes as described above. To screen for successful revertants, the *hdfR* and *yjfC* genes were PCR amplified (Table S5) and digested with *Ase*I and *Sac*I restriction enzymes, respectively. λ-Red recombineering was performed as described above with modifications to repair the mutated *pitA* gene using the *cat-sacB* selectable/counter-selectable cassette, as previously described.[49] The *cat-sacB* cassette was amplified from the *E. coli* TUC01 genome generously provided by Dr. Steven Kelly (Whitfield lab, University of Guelph), using PaCeR and primers that were designed to encompass regions immediately upstream and downstream of *pitA* (primers, Cat_pitA_Fwd/SacB_pitA_Rev; Table S5). The wild-type *pitA* gene was amplified using PaCeR (primers, pitA_76_Up/pitA_50_Low; Table S5). Recombinase-induced electrocompetent cells were transformed with 500 ng of the amplicon containing the *cat-sacB* cassette and grown overnight on LB containing chloramphenicol. Recombinase-induced electrocompetent cells of successful recombinants containing *cat-sacB* in the *pitA* region were then transformed with 2000 ng of the wild-type *pitA* amplicon and grown overnight on LB containing 6% (w/v) sucrose. Replacement of the cassette with the wild-type *pitA* gene was confirmed by the loss of resistance against chloramphenicol, growth on sucrose, and Sanger sequencing (The Center for Applied Genomics, SickKids or the Advanced Analysis Center, University of Guelph).

For the genomic integration of the 'Pore', the *fhuA ΔC/Δ4L* gene and an adjacent gentamicin resistance cassette were amplified from the genome of an *E. coli* K-12 str. BW25113 harboring the 'Pore' gene using PaCeR (primers, fhuA_40_Up/glmS_3680_Low; Table S5). Pore integration and removal of the resistance cassette were performed as described above using λ-Red recombineering. The pore was introduced into the intergenic region between *glmS* and *pstS* and verified using PCR (primers, pstS_520_Up/glmS_3680_Low, Table S5). The activity of the pore was confirmed through susceptibility testing with vancomycin, as described previously.[9]

Whole genome sequencing of Δ*tolC* and the TE mutant

Genomic DNA from the Δ*tolC* and TE mutants was extracted from overnight cultures using the PureLink Genomic DNA Mini Kit (Invitrogen) according to the manufacturer's suggested guidelines. Nanopore long-read DNA library preparation was performed using a PCR-free V14 chemistry ligation sequencing kit by SeqCenter (Pennsylvania, USA), and sequencing was performed on a MinION platform. Raw sequencing reads were assembled with the Flye *de novo* assembler,[59] then annotated with the *E. coli* K-12 str. BW25113 reference genome (accession no. CP009273.1) from NCBI using Geneious Prime v2020.2.4.[60] Whole genome sequencing data of the TE mutant containing the non-synonymous mutations were deposited in the GenBank database (BioProject ID PRJNA990483). For short-read sequencing, Illumina DNA library preparation was performed using an Illumina Nextera kit by SeqCenter (Pennsylvania, USA), followed by Illumina sequencing on a NextSeq 2000 platform. Low-quality reads were trimmed using an in-suite BBDuk plug-in and raw reads were aligned to the *E. coli* K-12 str. BW25113 reference genome with bowtie2. Genomic differences between the Δ*tolC* and TE mutant genomes relative to wild-type *E. coli* K-12 strain were identified using the following thresholds: minimum variant frequency of 0.75, maximum variant P-value of 10^{-6}, and minimum variant P-value of 10^{-5}. Breseq[61] was used to confirm the mutations identified using Geneious. Whole genome sequencing data of Δ*tolC* and the repaired TE mutant were also deposited in the GenBank database (BioProject ID PRJNA990483).

Generation of synthetic #20 resistant mutants

Resistance-conferring mutations in Δ*tolC* were generated using the single-step selection method.[62] Briefly, a single colony was inoculated into MHB II and grown overnight at 37°C with aeration (220 rpm). The overnight culture was diluted 1:10 in fresh MHB II and 180 μL of the diluted culture was applied to the surface of MHB II agar containing 4X the MIC of the compound of interest. The plates were incubated at 37°C for 48 h. Isolated colonies were patch-plated onto MHB II agar containing 4X MIC of the compound of interest, and the susceptibility level of the mutants was assessed using the CLSI broth microdilution method[63] in MHB II as described below.

Antimicrobial susceptibility testing

Minimum inhibitory concentrations (MICs) were determined using the CLSI broth microdilution method.[63] Briefly, strains were applied to LB agar and incubated overnight at 37°C. To prepare the inoculum, colonies were suspended in sterile 0.85% (w/v) NaCl to an OD_{600nm} of ~0.1, then diluted 1:100 in MHB II. In a round-bottom 96-well microtiter plate (VWR), compounds were serially titrated 2-fold in 50 μL of MHB II, followed by the addition of 50 μL of the diluted cell suspension, resulting in a final well volume of 100 μL. Plates were incubated at 37°C with aeration (900 rpm) for 18 h, and the OD_{600nm} was measured using a BioTek Synergy H1 microplate reader. Chequerboard assays were performed using the same methodology with modifications as described. Compound A was serially titrated 2-fold on the x axis while compound B was serially titrated 2-fold on the y axis. Cell inocula and final volumes remained at 50 μL and 100 μL, respectively.

RT-qPCR

The RT-qPCR procedure followed the MIQE Guidelines[64] for quality control. 3 mL of LB supplemented with spectinomycin and kanamycin was inoculated with a single colony and incubated at 37°C with aeration (220 rpm) for 18 h. To induce CRISPRi-mediated *msbA* knockdown using the pFD152 plasmid,[55,56] 3.125 μg/mL and 0.05 μg/mL of aTc, equivalent to 0.5x the MIC, were added to the wild-type K-12 and Δ*tolC* cultures, respectively, at the time of inoculation. Saturated overnight cultures were diluted with LB to an OD_{600nm} of 0.4. 1 mL of diluted cells were harvested by centrifugation at room temperature and total RNA was extracted using the RNeasy Mini Kit (Qiagen) according to the manufacturer's guidelines. RNA quality and quantity were determined using a Nanodrop 2000 Spectrometer (Thermo Fisher). The integrity of RNA samples was assessed by gel electrophoresis before cDNA synthesis. 400 ng of RNA was treated with the TURBO DNA-Free Kit (Invitrogen) according to the manufacturer's guidelines to degrade contaminating genomic DNA. The samples were reverse transcribed into cDNA using the Superscript IV First Strand Synthesis System Kit (Invitrogen) according to the manufacturer's guidelines. Primers were designed using the PrimerQuest Tool (IDT) to amplify ~100 bp products within the target gene and the endogenous reference gene (Table S5). *recA* was used as the reference gene to normalize transcript levels between samples.[65] A five-point, 10-fold serial dilution of cDNA was used to generate standard curves for the *msbA* and *recA* primer sets, which was performed to validate the qPCR primer efficiencies using the Powertrack SYBR Green Master Mix kit (Thermo Fisher Scientific) according to the manufacturer's guidelines. Reactions were set up in MicroAmp EnduraPlate Optical 96-Well Clear Reaction plates (Applied Biosystems) and amplified using the QuantStudio 3 Real-Time PCR System (Applied Biosystems). After amplification, a melt curve analysis was performed. The data were analyzed using the Design and Analysis Software from Thermo Fisher QuantiGene Plex Data Analysis (Version 2.6.2). The line of best fit for the *msbA* primer set was $y = -3.4361x + 24.678$ (R^2 = 0.996), with a primer efficiency calculated to be 95.4%. The line of best fit for the *recA* primer set was $y = -3.4817x + 22.523$ (R^2 = 0.998), with a primer efficiency calculated to be 93.6%. Upon satisfying the acceptable standard curve parameters (primer efficiency of 90–100%, slope between −3.58 and −3.10, and $R^2 > 0.99$),[64] the cDNA samples were diluted 1:100 before being used in RT-qPCR as described above.

Relative quantification was carried out and relative fold gene expression was calculated using the ΔΔCt method.[66] A negative reverse transcriptase control and no template controls for both primer sets were included in each RT-qPCR plate to ensure the absence of extraneous and genomic DNA contamination. Three technical replicates were used for each sample, and the results are representative of three independent biological replicates.

CRISPRi-mediated *msbA* repression

The effect of *msbA* CRISPRi-mediated repression on bacterial fitness was assessed using the CLSI broth microdilution method,[63] as described above with modifications. Strains harboring pFD152:*msbA* were propagated on LB agar supplemented with spectinomycin and kanamycin. Cell inocula were prepared as described above. The anhydrotetracycline (aTc) inducer was serially titrated 2-fold in 50 μL of MHB II in a round-bottom 96-well microtiter plate (VWR). Then, 50 μL of the diluted cell suspensions were applied to the plate. The microtiter plates were incubated at 37°C with aeration (900 rpm) for 24 h, and the OD_{600nm} was measured using a BioTek Synergy H1 microplate reader.

MsbA ATPase assay

The MsbA protein from *E. coli* was purified and reconstituted into amphipols as previously described.[18] MsbA ATPase activity was measured using a Transcreener ADP2 FP Assay (BellBrook Labs). To determine the IC_{50}, synthetic compound #20 was first incubated with 2× MsbA enzyme solution for 10 min and the reaction was initiated with 2× ATP solution. The final concentration of each reagent used in the assay was 9.2 nM of purified *E. coli* MsbA in amphipol, 50 μM ATP in 50 mM Tris (pH 7.5), 10 mM $MgCl_2$, 1% glycerol, 0.1% bovine gamma globulin, 1 mM dithiothreitol (DTT), 0.007% Brij-35 and 0.5% dimethyl sulfoxide (DMSO). Under these conditions, the typical and uninhibited ATPase activity for MsbA was 87 nmol min^{-1} mg^{-1}. To quench the reaction, Transcreener Detection Buffer was added when 5% of the ATP was hydrolyzed to ADP. The IC_{50} was determined by fitting the inhibition dose-response curve with a nonlinear four-parameter inhibition model (GraphPad Prism).

Thin-section transmission electron microscopy

A pellet of cultured bacteria was fixed in 1/2 Karnovsky's fixative (2% paraformaldehyde, 2.5% glutaraldehyde in 0.1M sodium cacodylate buffer, pH 7.2) and then post-stained with 1% reduced osmium tetroxide (OsO4). "En block" staining of samples was in 0.5% uranyl acetate. The bacteria were then dehydrated through a series of increasing ethanol concentrations, washed in propylene oxide, and then processed into epoxy resin (Eponate 12). The infiltrated samples were then polymerized at 65°C for two days. Ultrathin sections were prepared with an Ultracut microtome (Leica) and transferred to 75 mesh copper grids. Sections were stained with 0.2% lead citrate. Images were taken with a JEOL JEM-1400 TEM (transmission electron microscope) at 80keV and a GATAN Ultrascan 1000 CCD camera.

Outer membrane permeability assay

Strain permeability was evaluated using 1-*N*-phenylnaphthylamine (NPN) (Sigma-Aldrich) uptake assays. Overnight cultures grown in MHB II at 37°C for 18 h were subcultured to an OD_{600nm} of 0.1 in MHB II, then grown to an OD_{600nm} of 0.6 at 37°C. The cells were harvested and washed three times with phosphate-buffered saline (PBS) and resuspended in PBS to a final OD_{600nm} of 0.6. To disrupt efflux activity, 0.781 μg/mL, 6.25 μg/mL, and 12.5 μg/mL of carbonyl cyanide *m*-chlorophenyl hydrazone (CCCP), equivalent to 1x the MIC of each strain, was incubated with the cell suspensions of Δ*tolC*, EKO-35, and the TE mutant strains, respectively, at room temperature for 30 min. Solid black bottom 96-well microtiter plates (VWR) were blocked with 2% (w/v) bovine serum albumin (HyClone) for 15 min at room temperature. 180 μL of the cell inocula were then applied to the microtiter plates, followed by the addition of NPN at a final concentration of 1 μg/mL, resulting in a final well volume of 200 μL. Fluorescence was measured using a BioTek Synergy H1 microplate reader for 30 min using excitation and emission wavelengths of 350 nm and 420 nm, respectively.

Scanning electron microscopy

Saturated overnight cultures were diluted 1:100 in LB, supplemented with antibiotics when necessary, and grown at 37°C with aeration (220 rpm) until an OD600 nm of ~0.5 was achieved. When required, the subcultures were supplemented with 0.5x the MIC of synthetic compound #20 or aTc to determine the effects of MsbA inhibition and *msbA* repression, respectively, on cell morphology. For Δ*tolC*, 0.1563 μg/mL of synthetic compound #20, equivalent to 0.5x the MIC, was added. 1.5 mL of cultures in the mid-exponential growth phase were harvested by centrifugation, washed three times with sterile 0.85% (w/v) NaCl, and resuspended in 400 μL of 0.85% (w/v) NaCl. 200 μL of the cell suspension was applied to a carbon planchette (Ted Pella) and incubated at room temperature for 30 min. The cell suspension was removed and the planchettes with adhered cells were submerged in 2% glutaraldehyde (v/v) for 30 min, then washed three times with 0.85% (w/v) NaCl. The planchettes were then submerged in 1% (v/v) osmium tetraoxide for 30 min and then washed once with 0.85% (w/v) NaCl. The cells were dehydrated in a graded ethanol series, and then fully dried using a Denton DCP-1 critical point dryer. Samples were coated immediately with 15 nm of gold using a sputter coater (Denton Desk V TSC). Images were acquired using an FEI Quanta FEG 250 scanning electron microscope (Thermo Fisher Scientific) operated at 20.0 kV under high vacuum at the Molecular and Cellular Imaging Facility (University of Guelph). ImageJ (Fiji)[58] was used to measure cell lengths.

Atomic force microscopy

AFM experiments were performed in PBS at room temperature using a JPK NanoWizard 4 NanoScience Instrument. Overnight cultures were diluted 1:100 in LB and grown at 37°C with aeration (220 rpm) until the mid-exponential phase of growth (OD_{600nm} = ~0.5) was achieved. The cells were then harvested by centrifugation and washed three times in PBS. A 100x diluted bacterial suspension was left to adhere to poly-ethylenimine (PEI)-coated glass bottom dishes for 1 h, then gently rinsed three times with PBS before AFM measurements. AFM cantilevers were calibrated by the thermal noise method.[67] Imaging was performed in quantitative (QI) mode using SNL-10 cantilevers. Height images were recorded at a constant approach/retract speed of 25 μm/s, using an applied force of 0.25 nN and a ramp size of 500 nm. Cell surface morphology parameters (height, roughness, length, and volume) were extracted from height images acquired at low resolution (128 × 128 pixels^2 on 8 × 8 μm^2 areas) or high-resolution (256 x 256 pixels^2 on 200 × 200 nm^2 areas on top of the bacteria). For the mechanical characterization of strains, force-indentation curves were recorded in force-volume mode (16 curves × 16 curves) in 250 × 250 nm^2 regions on top of the cells. Curves were recorded using MSCT-E cantilevers, using an applied force of 1 nN, a constant approach/retract speed of 1 μm/s, and a ramp size of 1 μm. The approach segment of the force-distance curves was fitted with the Hertz/Sneddon model over a distance of 20 nm, using a Poisson ratio of 0.5 and considering a conical tip of 17.5° half-cone angle.[68] Young's Modulus (E) was extracted from the nonlinear region of the curves and the spring constant (k) was calculated through the slope of their linear region. For each cell, these values were plotted as histograms and the average values were extracted by fitting with a Gaussian function. Statistical analysis was carried out using Origin software (OriginPro 2021), applying a statistical Tukey's multiple-comparison test. Data were analyzed with JPK Data Processing software.

QUANTIFICATION AND STATISTICAL ANALYSIS

Statistical analyses were conducted using GraphPad Prism 9.4.1, Excel 16.36, and OriginPro 2021. Data obtained from qRT-PCR experiments were analyzed using the Thermo Fisher QuantiGene Plex Data Analysis (Version 2.6.2). Detailed information regarding statistical methods for each experiment can be found in the figure legends and the corresponding figures.